

Heterozygous nonsense variants in laminin subunit 3 α resulting in Ebstein's anomaly

Zhou Zhou,^{1,7} Xumei Huang,^{2,7} Xia Tang,^{3,7} Wen Chen,¹ Qianlong Chen,¹ Chaohui Zhang,⁴ Yuxin Li,⁴ Dachun Zhao,⁵ Zhe Zheng,¹ Shengshou Hu,¹ Jikui Wang,^{4,*} Iftikhar J. Kullo,⁶ and Keyue Ding^{6,8,*}

Summary

Ebstein's anomaly is a rare congenital heart disease characterized by tricuspid valve downward displacement and is associated with additional cardiac phenotypes such as left ventricle non-compaction. The genetic basis of Ebstein's anomaly has yet to be fully elucidated, although several genes (e.g., *NKX2-5*, *MYH7*, *TPM1*, and *FLNA*) may contribute to Ebstein's anomaly. Here, in two Ebstein's anomaly families (a three-generation family and a trio), we identified independent heterozygous nonsense variants in laminin subunit 3 α (*LAMA3*), cosegregated with phenotypes in families with reduced penetrance. Furthermore, knocking out *Lama3* in mice revealed that haploinsufficiency of *Lama3* led to Ebstein's malformation of the tricuspid valve and an abnormal basement membrane structure. In conclusion, we identified a novel gene-disease association of *LAMA3* implicated in Ebstein's anomaly, and the findings extended our understanding of the role of the extracellular matrix in Ebstein's anomaly etiology.

Ebstein's anomaly (MIM: 224700) is a rare congenital heart disease characterized by the failure of tricuspid valve leaflets to separate from the ventricular wall.¹ As a result, the septal and/or the posterior leaflets of the tricuspid valve are displaced apically, leading to atrialization of the right ventricle (RV). Ebstein's anomaly often accompanies additional cardiac phenotypes, including structural abnormalities and accessory conduction pathways.¹ We have previously classified Ebstein's anomaly into three groups based on human phenotype ontology (HPO)-standardized phenotypes associated with Ebstein's anomaly.² There is a birth prevalence of 61 cases per million infants and 1 of 200,000 live births.^{1,3} Analysis of the inheritance mode in familial Ebstein's anomaly suggested a genetic component inherited as a polygenic character with a threshold phenomenon.⁴ Several genes (e.g., *NKX2-5* [MIM: 600584],⁵ *MYH7* [MIM: 160760],⁶ *TPM1* [MIM: 191010],⁷ and *FLNA* [MIM: 300017]⁸) may contribute to Ebstein's anomaly, which is associated with additional cardiac (e.g., left ventricle non-compaction [LVNC]) or extracardiac phenotypes (Table S1). With variable expressiveness and reduced penetrance,⁹ Ebstein's anomaly is one of the least understood congenital heart diseases, and its genetic basis remains largely unknown.

A three-generation family of five individuals (pedigree_w) was collected at the Department of Cardiovascular Diseases, Wenzhou Central Hospital (Wenzhou, China) as was a second trio (trio_p) from the Department of Cardiovascular

Diseases, Fuwai Hospital of Chinese Academy of Medical Sciences (Beijing, China). In pedigree_w, the proband (III1) was diagnosed by fetal echocardiography (Figure 1A) during a routine prenatal examination when the mother (II2) was at 26-week gestation. The diagnosis was further confirmed by postnatal transthoracic echocardiography (TTE) (Figure 1B). TTE for the mother was consistent with Ebstein's anomaly (Figure 1C). We did not find other anomalies (e.g., LVNC) in the affected individuals. The mother had no history of valproate, carbamazepine, lithium, lamotrigine, antipsychotic, or antidepressant drug use. In trio_p (Figure 1D), the proband (III1) was a 2-year-old female found to have a cardiac murmur via routine physical examination. Echocardiography showed displacement of the septal leaflet, an absent posterior leaflet, and an enlarged right atrium (Figure 1E). The clinical features of the two families are summarized in Figure 1F. There was no evidence of Ebstein's anomaly in the grandparents in pedigree_w (I1 and I2) or the parents in trio_p (I1 and I2). Therefore, we assumed either an autosomal-dominant (AD) (inheritance with reduced penetrance) or a *de novo* model in both families for further inheritance pattern analysis. The enrolled members in both families reported no additional cardiac symptoms, and no further segregation was observed. The families provided written informed consent, and the procedure of this study followed ethical standards. This study was approved by the Institutional Review Board (IRB) at each site that recruited the individuals.

¹Department of Laboratory Medicine, State Key Laboratory of Cardiovascular Disease, Fuwai Hospital, National Center for Cardiovascular Diseases, Chinese Academy of Medical Sciences and Peking Union Medical College, Beijing 100037, P.R. China; ²Department of Cardiovascular Diseases, Wenzhou Central Hospital, Wenzhou, Zhejiang 325000, P.R. China; ³State Key Laboratory of Genetic Engineering and Collaborative Innovation Center for Genetics and Development, School of Life Sciences, Fudan University, Shanghai 200433, P.R. China; ⁴Henan Key Laboratory of Medical Tissue Regeneration, Xinxiang Medical University, Xinxiang, Henan 453003, P.R. China; ⁵Department of Pathology, Peking Union Medical College Hospital, Chinese Academy of Medical Sciences and Peking Union Medical College, Beijing 100730, P.R. China; ⁶Department of Cardiovascular Medicine, Mayo Clinic, Rochester, MN 55905, USA

⁷These authors contributed equally

⁸Lead contact

*Correspondence: wjk@xxmu.edu.cn (J.W.), ding.keyue@mayo.edu (K.D.)

<https://doi.org/10.1016/j.xhgg.2023.100227>.

© 2023 The Author(s). This is an open access article under the CC BY-NC-ND license (<http://creativecommons.org/licenses/by-nc-nd/4.0/>).



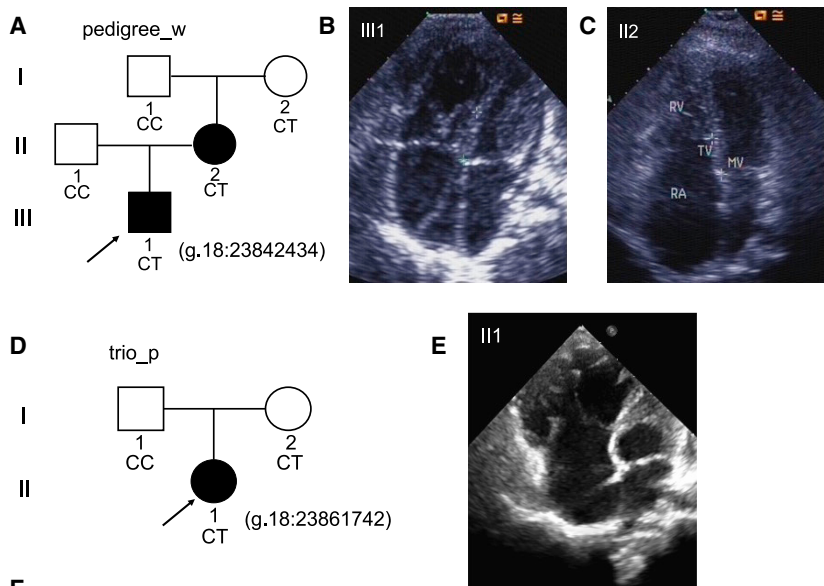


Figure 1. The collected two families with Ebstein's anomaly

(A) The family structure of pedigree_w. (B) Apical 4-chamber view in the proband III1 exhibited an apical displacement of the tricuspid valve. (C) Apical 4-chamber view in II2 showed similar phenotypes to the proband III1. (D) A trio (trio_p). (E) Apical 4-chamber view in II1. (F) Clinical characteristics of the two Ebstein's anomaly families. LV non-compaction, atrial septal defect, atrial arrhythmias, bundle branch block, cyanosis, cardiomegaly, fatigue, and dyspnea were not noted.

variants in AD, and seven *de novo* variants in trio_p, respectively. Two genes were prioritized in both families, i.e., *LAMA3* (laminin subunit 3 α) (MIM: 600805) and *APOL4* (apolipoprotein L4). We excluded *APOL4* since the frameshift variant (g.22:36191797ACT>A) identified in both families was located within a common microsatellite (https://www.ncbi.nlm.nih.gov/clinvar/variation/445778/?new_evidence=true). In *LAMA3*, two independent heterozygous nonsense variants were identified, including p.Arg1126Ter (GenBank: NP_001121189.2) (g.18:23842434C > T) in pedigree_w and p.Gln1507Ter (g.18:23861742C > T) in trio_p, respectively.

Whole-genome sequencing for five individuals in pedigree_w was conducted on an Illumina HiSeq 4000, generating 234–248 GB paired-end sequencing data with a depth of approximately $32\text{--}33\times$. For trio_p, whole-exome sequencing libraries were constructed using Agilent SureSelect Human All Exon V4+UTRs and were sequenced on the Illumina HiSeq 2000 (paired-end 100-bp reads). Sequencing reads were aligned to the human reference genome (GRCh38) with Burrows-Wheeler Aligner (BWA), followed by duplicate removal and base score quality recalibration. Single-nucleotide variants (SNVs) and small insertions and deletions (indels) were called using DeepVariant (v.1.4).¹⁰ We used the Ensemble Variant Effect Predictor (VEP; v.98)¹¹ to annotate variants. A “rare variant” was defined as having a maximal global and East Asian frequency of 0.001 or as not being identified in the 1000 Genome Project (1000G)¹² and the Genome Aggregation Database (gnomAD).¹³ We classified functional variants using the subjective classification of the severity of the variant consequence (IMPACT) and classifications from PolyPhen and SIFT. Variants with IMPACT high or moderate and SIFT matching deleterious or PolyPhen matching damaging were considered functional variants.

Using a vigorous filtering pipeline (Figure 2A), we finalized 58 variants consistent with the AD model in pedigree_w, 112

These two rare loss-of-function (LoF) variants (with global frequencies of 2×10^{-5} and 1.6×10^{-5} in gnomAD, respectively) cosegregated with the phenotypes but with reduced penetrance, as the unaffected I2 in both families was a carrier, which was confirmed by Sanger sequencing (Figures 2B and 2D). These LoF variants located in conserved regions across different species (Figures 2C and 2E). The identified LoF variants in both families and pathogenic/like pathogenic predicted LoF variants characterized from gnomAD¹³ were mainly distributed in the laminin EGF-like and G-like domains (Figure 2F). A pLI (the probability of being LoF intolerant¹⁴) of 0 and a LOEUF (the LoF observed/expected upper bound fraction¹³) of 0.691 derived from gnomAD suggested that *LAMA3* might not have a strictly selective constraint. Although both nonsense variants were classified into “variants of uncertain significance (VUSs)” by Clinvar,¹⁵ Intervar¹⁶ classified them into “pathogenic” with evidence of “PVS1, PM2, and PP3” according to the ACMG/AMP criteria.¹⁷ Phred-like combined annotation dependent depletion (CADD) scores¹⁸ of 35 and 43 in these two nonsense variants corresponded to the top 0.0316% and 0.005% of CADD scores from ~8.6 billion SNVs in the human genome, respectively. A CADD score ≥ 28.1 was considered “PP3 moderate” based on the

Characteristics	pedigree_w					trio_p		
	III1 (M)	II1 (M)	II2 (F)	I1 (M)	I2 (F)	II1 (F)	I1 (M)	I2 (F)
Age	8 mo	29 y	27 y	50 y	50 y	2 y	37 y	36 y
Displacement of the tricuspid valve	+	-	+	-	-	+	-	-
Atrialization of RV	+	-	+	-	-	+	-	-
Tricuspid regurgitation	+	-	+	-	-	+	-	-
LV ejection fraction	82%	68%	68%	65%	72%	67%	66%	68%
Murmur	+	-	+	-	-	+	-	-
Blood pressure (mmHg)	NA	110/70	104/68	132/80	130/82	91/51	NA	NA

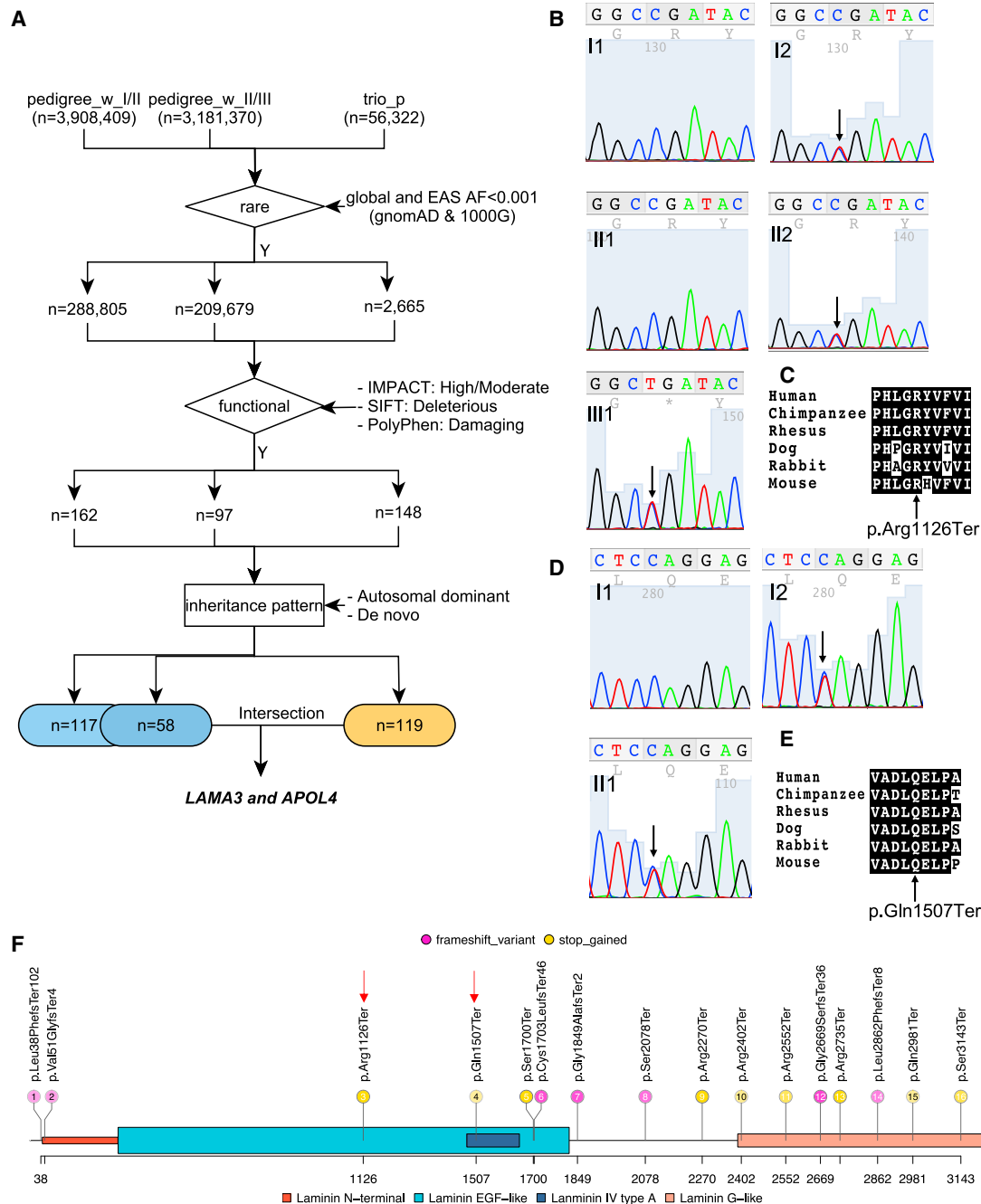


Figure 2. Nonsense variants in *LAMA3* were identified in the two Ebstein’s anomaly families

(A) A rigorous variants filtering flowchart prioritized *LAMA3*. We analyzed pedigree_w in two trios separately (pedigree_w_I/II and pedigree_w_II/III).

(B) Sanger sequencing confirmed the nonsense variant (p.Arg1126Ter [GenBank: NP_001121189.2] [g.18:23842434C>T]; indicated by an arrow) identified in pedigree_w. LoF, loss of function.

(C) Conservation of the LoF variant among different species.

(D) Sanger sequencing confirmed the nonsense variant (p.Gln1507Ter [g.18:23861742C>T]) identified in trio_p.

(E) Conservation of the LoF variants in different species.

(F) The pathogenic or like pathogenic predicted LoF variants in gnomAD distributed in different domains in *LAMA3*, along with two LoF variants (red arrow) identified in the present study. Seven pathogenic/like pathogenic pLOF variants in splicing site annotated in gnomAD were not shown.

calibrated recommendation for PP3 evidence,¹⁹ as the evidence for “pathogenic” classification used *in silico* tools.

We did not identify rare functional variants in the known genes implicated in Ebstein’s anomaly (Table S1) and could

not prioritize candidate genes using a phenotype-driven method (e.g., *Exomiser*^{20,21}). To identify underlying copy-number variants (CNVs), we performed high-density genotyping using the Infinium OmniExpressExome-8 v.1.3

BeadChip (958,497 markers) (Illumina, San Diego, CA, USA) in pedigree_w. We obtained an average call rate of 99.94% using the quality control implemented previously.²² We screened for chromosomal abnormalities from the family by analyzing B allele frequency and any areas where the log *R* ratio deviated from zero using PennCNV.²³ A joint CNV-calling algorithm was used for two parent-offspring trios separately. We also used CNVnator²⁴ to detect CNVs of various sizes based on read depth from the whole-genome sequencing data. After filtering, 228 PennCNV- and 94 CNVnator-predicted CNVs were retained (Tables S2 and S3). In trio_p, whole-exome-sequencing-based CNV was called using cn.mops,²⁵ which was filtered if it was <10 kb or if it overlapped with common CNVs (>35%) in the Database of Genomic Variants (DGV). Of note, only four regions have a fraction of reciprocal overlap (i.e., concordant > 0.50) (Table S4). These results suggested that CNVs may not play causal roles on these families.

Previous studies have shown that variants in extracellular matrix (ECM) components (e.g., laminin, integrin, collagen, and plectin) are associated with different forms of epidermolysis bullosa (EB) in autosomal recessive mode,^{26,27} with an estimated prevalence of 11 per million population over a 16-year period.²⁸ LAMA3, a member of the laminin 332 complex, is essential for maintaining the integrity of the basement membrane (e.g., collagen chain trimerization), MET promotes cell motility and cell junction organization. A proportion of 9% of patients with junctional EB (an incidence of 2.7 per million live births²⁸) were caused by homozygous pathogenic variants in LAMA3 (<https://www.ncbi.nlm.nih.gov/books/NBK1125>).²⁹ Although cardiac phenotypes in carriers of the junctional EB families harboring LAMA3 pathogenic variants have not been reported, patients with EB have been associated with various cardiac phenotypes, including bicuspid aortic valve,³⁰ LVNC and aortopathy,^{31,32} dilated cardiomyopathy,^{33–36} and atrial fibrillation.³⁷ Kur-nicka et al.³⁰ showed significantly aberrant RV diastolic function (including the maximal velocity of the atrial wave and tricuspid annulus late diastolic velocity) in 23 patients with EB. These observations suggested the potential association of LAMA3 with Ebstein's anomaly.

We thus hypothesized that LoF mutations in LAMA3 might alter the structure and function of laminin α 3 and thus change its ability to form heterotrimeric laminins. We investigated the potential roles of *Lama3* in the developing cardiac valves of *Lama3* knockout (KO) mice. The supplemental methods provide a detailed description of the experimental procedures for analyzing *in vivo* CRISPR-Cas9-mediated *Lama3* KO mice. *Lama3* was expressed in the mouse heart at the embryonic day 17.5 (E17.5) and postnatal day 3 (P3) stages, as well as in valves at E17.5 (Figure 3A). We investigated cardiac phenotypes in the sectioned hearts from E18.5, P1, and adult mice. The phenotypic analysis confirmed the roles of *Lama3* in the delamination and/or remodeling of the tricuspid valve leaflets. Compared with the wild type (Figure 3B), a *Lama3*^{+/-} mouse at E18.5 (Figure 3C) showed an elongation of both tricuspid mural (tml) and septal (tsl) leaflets

and an incomplete delamination of tmls from the RV wall. A P1 neonatal mouse exhibited a downward displacement of the annulus fibrosus, leading to an increased right atrium and a decreased RV (i.e., atrialization of RV) (Figure 3D). In a coronal plane section, compared with a control mouse (Figure 3E), a *Lama3*^{+/-} adult mice showed a downward displacement of the annulus fibrosus of the tricuspid valve (Figure 3F). In addition to abnormal elongation of the tricuspid valve leaflets and a failure of separation, homozygous deletion of *Lama3* led to either a thin ventricular wall and an enlarged RV cavity (Figure 3G) or a thickened wall and a reduced RV cavity (Figure 3H). All *Lama3*^{-/-} mice were aborted or died immediately after birth, supporting the hypothesis of the intolerant of homozygous LoF variants in *Lama3*. Our results showed that *Lama3* deficiency results in abnormalities in the tricuspid valve and RV, similar to phenotypes observed in human Ebstein's anomaly.

We further assessed whether the *Lama3* mice had an abnormal basement membrane of the tricuspid valve at the ultrastructural level. Compared with the control mice (Figure 4A), interstitial cells in KO mice were significantly stretched and showed an increased expression of collagens (Figure 4B). On the atrial side, the basement membrane of the tricuspid valve in the control mice was constrained by collagen fibrils and interstitial cells (Figure 4C). However, in the KO mice, the basement membrane appeared considerably thinned (Figure 4D) and/or disorganized (Figure 4E), suggesting a limited binding of laminin with integrin and collagen due to the *Lama3* deficiency. We also noted a thinning basement membrane on the ventricular side (Figures 4F and 4G). These results demonstrated that laminin deficiency affected the integrity of the basement membrane. A normal electrocardiogram (ECG) in control and KO mice by electrocardiogram recording suggested that *Lama3* deficiency did not lead to an accessory conduction system (Figure S1).

Our efforts to identify the genetic basis of Ebstein's anomaly showed a novel gene-disease association that independent heterozygous nonsense variants identified in LAMA3 in two families (Figures 1 and 2). Potentially novel gene-disease associations in rare diseases are increasingly being ascertained through recurrent cases, whereas it may not be sufficient to prove disease causality.³⁸ Our phenotypic analysis of *Lama3* KO mice showed abnormal tricuspid valves of downward displacement and/or elongation of the leaflets (i.e., like human Ebstein's anomaly) (Figure 3), as well as an abnormal basement membrane underlying the tricuspid valve (Figure 4), implying that the aberrant structure and function of the ECM resulting from *Lama3* haploinsufficiency may contribute to Ebstein's anomaly pathogenesis. The ECM influences cell signaling and functional outcomes in cardiac valve development³⁹; for example, atrioventricular canal (AVC) cardiomyocytes contribute to the development of tmls via ECM-cardiomyocyte interaction.⁴⁰ The basement

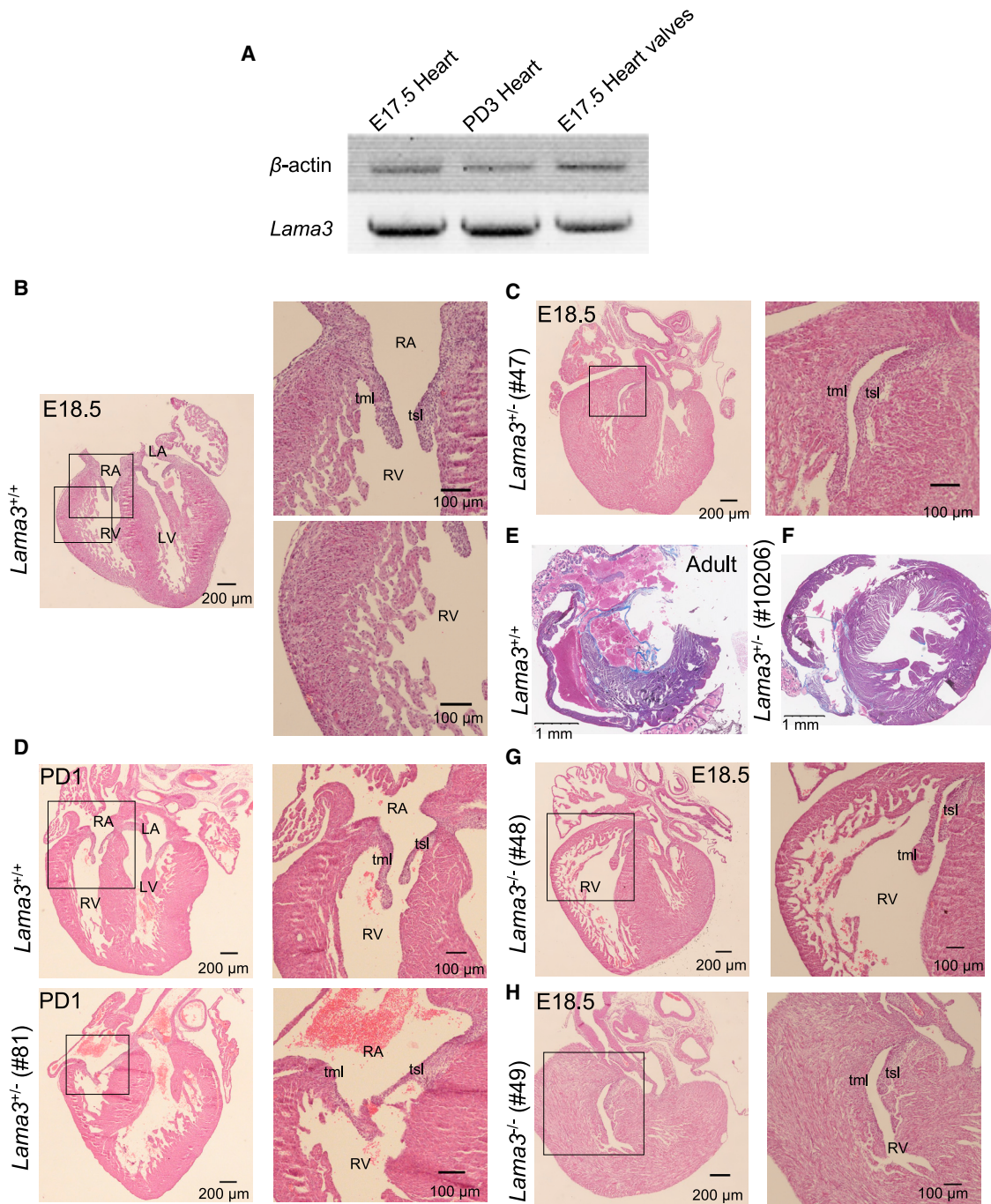


Figure 3. Histological analysis of *Lama3* knockout (KO) mice

(A) Expression of *Lama3* in the developing mouse fetal (E17.5) heart and valves, as well as postnatal day 3 (P3) heart.

(B) H&E staining of a control mouse at E18.5 with magnifications of the tricuspid valve and RV.

(C) In an E18.5 *Lama3*^{+/-} mouse, H&E staining revealed a delamination failure of the tricuspid mural leaflet (tml).

(D) A *Lama3*^{+/-} mouse at P1 demonstrated a downward displacement of the annulus fibrosus and an incomplete separation of the tricuspid septal leaflet (tsl).

(E and F) A coronal section (Masson's trichrome staining) of the heart in a control adult (E) and *Lama3*^{+/-} mouse (F). Muscles appear black, and fibers appear blue. A *Lama3*^{+/-} mouse showed that the annulus fibrosus of the tricuspid valve is equal to the mitral annulus. In contrast, a *Lama3*^{+/-} mouse showed RV hypertrophy and only the tricuspid valve tendinous cord at the mitral annulus remained, indicating a downward displacement of tricuspid annulus fibrosus.

(G and H) Abnormal staining of the tricuspid valve and right ventricular wall in *Lama3*^{-/-} mice at E18.5, showing either hypoplasia (G) or hypertrophy (H) of the RV.

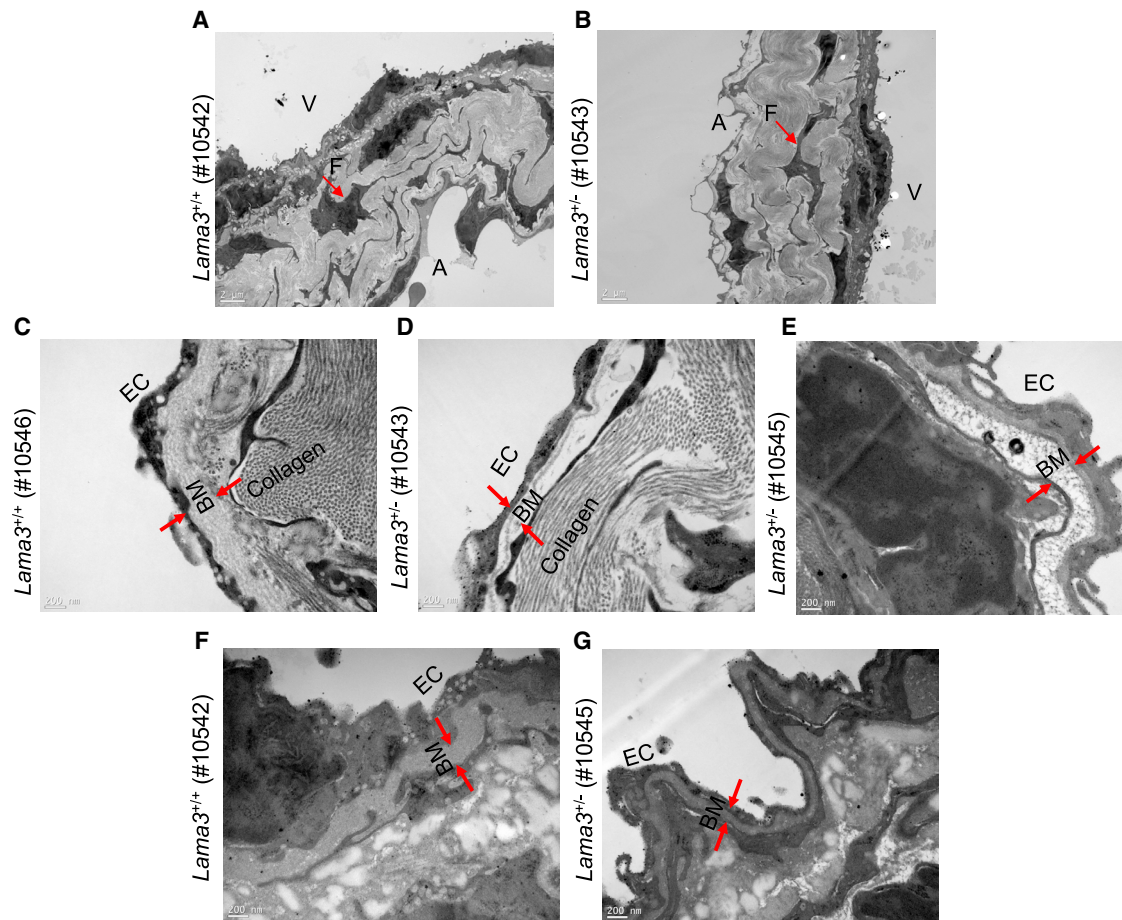


Figure 4. Transmission electron micrographs of tricuspid valve basement membranes in the *Lama3*^{+/-} mouse line and control littermates

(A and B) Low-magnification micrograph of the tricuspid valve of a wild-type littermate and *Lama3*^{+/-} mouse (7 weeks old). EC—the endothelial cell layer—covers both the leaflet’s atrial (A) and ventricular (V) sides. The atrial side of the tricuspid valve leaflet is a monolayer of the endothelium. Interstitial cells, e.g., fibroblast-like cells, are scattered in the leaflet. F indicates Collagen.

(C–E) Basement membranes of the atrial side of the tricuspid valve leaflet from wild-type (C) and *Lama3*^{+/-} (D and E) mouse.

(F and G) Basement membranes (BM) of the ventricular side of the tricuspid valve leaflet from a wild-type (F) and a *Lama3*^{+/-} (G) mouse.

membrane—a highly organized network of the ECM—mainly comprises laminin, type IV collagen, and proteoglycans and underlies valve endothelial cells⁴¹ and surrounds cardiomyocytes.⁴² Self-assembly of the basement membrane network provides structural support for valve endothelial cells and is crucial for forming the cardiac sarcomere.⁴³ Dysregulation of the basement membrane composition and structure contributes to multiple pathological conditions, including non-compaction cardiomyopathy and abnormal leaflet elongation. Laminins are essential for basement membrane assembly and formation, playing a critical role in cell adhesion, collagen assembly, and receptor interactions during heart valve morphogenesis. A lack of laminins in the basement membrane may lead to a compensatory deposition of other ECM components (e.g., collagen), resulting in the thickening and elongation of the leaflets (and thus failure of delamination of the leaflets). An example supporting this hypothesis is, in Alport syndrome (MIM: 301050), the absence of collagen 4 α (3,4,5) may stimulate the reap-

pearance and abnormal accumulation of laminin-1 and lead to thickening and delamination.⁴⁴

We acknowledge several limitations in the present study. First, further studies including a large cohort of participants with Ebstein’s anomaly would enable rare functional enrichment analysis for genes involved in ECM components. Second, the qualitative representation provided valuable insights into the morphological alterations (Figures 3 and 4). Obtaining precise quantitative measurements for the phenotypes poses technical and practical challenges. The currently available imaging modalities may lack the necessary resolution and sensitivity to capture detailed measurements of the mouse embryo heart. While high-resolution echocardiography has been successfully used to accurately detect RV function in a mouse model of pulmonary hypertension,⁴⁵ achieving accurate visualization and quantification for the tricuspid valve remains technically demanding. In human tricuspid valve disease evaluation, three-dimensional echocardiography has been increasingly utilized to visualize tricuspid leaflet morphology and assess the level of leaflet attachment.⁴⁶

Although we acknowledge that accurate quantitative data would further support our qualitative findings and strengthen our conclusions, the utilization of such advanced technology is beyond the scope of the present study.

In conclusion, we identified a novel gene-disease association for Ebstein's anomaly and demonstrated that haploinsufficiency in *LAMA3* affects basement membrane components in Ebstein's anomaly pathogenesis.

Data and code availability

All the data described in this study are included in the main manuscript and in the [supplemental information](#).

Supplemental information

Supplemental information can be found online at <https://doi.org/10.1016/j.xhgg.2023.100227>.

Acknowledgments

The study was supported by CAMS Initiative for Innovative Medicine (CAMS-I2M) (no. 2016-I2M-1-016, Z. Zhou), Beijing Science & Technology innovation base cultivating and developing special project (no. Z151100001615054, Z. Zhou), a Research Startup Fund (no. 050510, J.W.), the Key Science and Technology Project of Henan (no. 182102310173, J.W.), and the National Natural Science Foundation of China (82170237, J.W.).

Author contributions

Z. Zhou, X.H., W.C., and Q.C., recruited the family and prepared samples; K.D. and X.T. performed data analysis; C.Z., Y.L., J.W., and D.Z. performed phenotypic analysis on KO mice. W.C. performed transmission electron microscopy (TEM) and ECG experiments. Z. Zheng, Z. Zhou, S.H., and J.W. provided funding support. I.J.K. commented on and revised the manuscript. K.D. wrote the paper with input from all authors. Z. Zhou, J.W., and K.D. supervised and designed the project.

Declaration of interests

The authors declare no competing interests.

Received: March 27, 2023

Accepted: July 26, 2023

Web resources

Database of Genomic Variants (DGV), <https://dgv.tcag.ca/dgv/app/home>.

DeepVariant, <https://github.com/google/deepvariant>.

Ensembl Variant Effect Predictor (VEP), <https://www.ensembl.org/info/docs/tools/vep/index.html>.

Online Mendelian Inheritance in Man, <http://www.omim.org>.

The Genome Aggregation Database (gnomAD), <https://gnomad.broadinstitute.org>.

The 1000 Genome Project, <https://internationalgenome.org>.

References

1. Attenhofer Jost, C.H., Connolly, H.M., Dearani, J.A., Edwards, W.D., and Danielson, G.K. (2007). Ebstein's Anomaly. *Circulation* *115*, 277–285. <https://doi.org/10.1161/circulationaha.106.619338>.
2. Tang, X., Chen, W., Zeng, Z., Ding, K., and Zhou, Z. (2020). An ontology-based classification of Ebstein's anomaly and its implications in clinical adverse outcomes. *Int. J. Cardiol.* *316*, 79–86. <https://doi.org/10.1016/j.ijcard.2020.04.073>.
3. van der Bom, T., Zomer, A.C., Zwinderman, A.H., Meijboom, F.J., Bouma, B.J., and Mulder, B.J.M. (2011). The changing epidemiology of congenital heart disease. *Nat. Rev. Cardiol.* *8*, 50–60. <https://doi.org/10.1038/nrcardio.2010.166>.
4. Rosenmann, A., Arad, I., Simcha, A., and Schaap, T. (1976). Familial Ebstein's anomaly. *J. Med. Genet.* *13*, 532–535. <https://doi.org/10.1136/jmg.13.6.532>.
5. Benson, D.W., Silberbach, G.M., Kavanaugh-McHugh, A., Cottrill, C., Zhang, Y., Riggs, S., Smalls, O., Johnson, M.C., Watson, M.S., Seidman, J.G., et al. (1999). Mutations in the cardiac transcription factor NKX2.5 affect diverse cardiac developmental pathways. *J. Clin. Invest.* *104*, 1567–1573. <https://doi.org/10.1172/jci8154>.
6. Postma, A.V., van Engelen, K., van de Meerakker, J., Rahman, T., Probst, S., Baars, M.J.H., Bauer, U., Pickardt, T., Sperling, S.R., Berger, F., et al. (2011). Mutations in the sarcomere gene MYH7 in Ebstein Anomaly. *Circ. Cardiovasc. Genet.* *4*, 43–50. <https://doi.org/10.1161/circgenetics.110.957985>.
7. Kelle, A.M., Bentley, S.J., Rohena, L.O., Cabalka, A.K., and Olson, T.M. (2016). Ebstein anomaly, left ventricular non-compaction, and early onset heart failure associated with a de novo α -tropomyosin gene mutation. *Am. J. Med. Genet.* *170*, 2186–2190. <https://doi.org/10.1002/ajmg.a.37745>.
8. Mercer, C.L., Andreoletti, G., Carroll, A., Salmon, A.P., Temple, I.K., and Ennis, S. (2017). Familial Ebstein Anomaly. *Circ. Cardiovasc. Genet.* *10*, e001683. <https://doi.org/10.1161/circgenetics.116.001683>.
9. Prendiville, T., Jay, P.Y., and Pu, W.T. (2014). Insights into the genetic structure of congenital heart disease from human and murine studies on monogenic disorders. *Cold Spring Harb. Perspect. Med.* *4*, a013946. <https://doi.org/10.1101/cshperspect.a013946>.
10. Poplin, R., Chang, P.-C., Alexander, D., Schwartz, S., Colthurst, T., Ku, A., Newburger, D., Dijamco, J., Nguyen, N., Afshar, P.T., et al. (2018). A universal SNP and small-indel variant caller using deep neural networks. *Nat. Biotechnol.* *36*, 983–987. <https://doi.org/10.1038/nbt.4235>.
11. McLaren, W., Gil, L., Hunt, S.E., Riat, H.S., Ritchie, G.R.S., Thormann, A., Flicek, P., and Cunningham, F. (2016). The ensembl variant effect predictor. *Genome Biol.* *17*, 122. <https://doi.org/10.1186/s13059-016-0974-4>.
12. 1000 Genomes Project Consortium, Auton, A., Brooks, L.D., Durbin, R.M., Garrison, E.P., Kang, H.M., Korbel, J.O., Marchini, J.L., McCarthy, S., McVean, G.A., and Abecasis, G.R. (2015). A global reference for human genetic variation. *Nature* *526*, 68–74. <https://doi.org/10.1038/nature15393>.
13. Karczewski, K.J., Francioli, L.C., Tiao, G., Cummings, B.B., Alfoldi, J., Wang, Q., Collins, R.L., Laricchia, K.M., Ganna, A., Birnbaum, D.P., et al. (2020). The mutational constraint spectrum quantified from variation in 141,456 humans. *Nature* *581*, 434–443. <https://doi.org/10.1038/s41586-020-2308-7>.

14. Fuller, Z.L., Berg, J.J., Mostafavi, H., Sella, G., and Przeworski, M. (2019). Measuring intolerance to mutation in human genetics. *Nat. Genet.* *51*, 772–776. <https://doi.org/10.1038/s41588-019-0383-1>.
15. Landrum, M.J., Lee, J.M., Benson, M., Brown, G.R., Chao, C., Chitipiralla, S., Gu, B., Hart, J., Hoffman, D., Jang, W., et al. (2018). ClinVar: improving access to variant interpretations and supporting evidence. *Nucleic Acids Res.* *46*, gkx1153. <https://doi.org/10.1093/nar/gkx1153>.
16. Li, Q., and Wang, K. (2017). InterVar: clinical interpretation of genetic variants by the 2015 ACMG-AMP guidelines. *Am. J. Hum. Genet.* *100*, 267–280. <https://doi.org/10.1016/j.ajhg.2017.01.004>.
17. Richards, S., Aziz, N., Bale, S., Bick, D., Das, S., Gastier-Foster, J., Grody, W.W., Hegde, M., Lyon, E., Spector, E., et al. (2015). Standards and guidelines for the interpretation of sequence variants: a joint consensus recommendation of the American College of Medical Genetics and Genomics and the Association for Molecular Pathology. *Genet. Med.* *17*, 405–424. <https://doi.org/10.1038/gim.2015.30>.
18. Kircher, M., Witten, D.M., Jain, P., O’Roak, B.J., Cooper, G.M., and Shendure, J. (2014). A general framework for estimating the relative pathogenicity of human genetic variants. *Nat. Genet.* *46*, 310–315. <https://doi.org/10.1038/ng.2892>.
19. Pejaver, V., Byrne, A.B., Feng, B.-J., Pagel, K.A., Mooney, S.D., Karchin, R., O’Donnell-Luria, A., Harrison, S.M., Tavtigian, S.V., Greenblatt, M.S., et al. (2022). Calibration of computational tools for missense variant pathogenicity classification and ClinGen recommendations for PP3/BP4 criteria. *Am. J. Hum. Genet.* *109*, 2163–2177. <https://doi.org/10.1016/j.ajhg.2022.10.013>.
20. Robinson, P.N., Köhler, S., Oellrich, A., Sanger Mouse Genetics Project, Wang, K., Mungall, C.J., Lewis, S.E., Washington, N., Bauer, S., Seelow, D., Krawitz, P., et al. (2014). Improved exome prioritization of disease genes through cross-species phenotype comparison. *Genome Res.* *24*, 340–348. <https://doi.org/10.1101/gr.160325.113>.
21. Wang, Q., Tang, X., Yang, K., Huo, X., Zhang, H., Ding, K., and Liao, S. (2022). Deep phenotyping and whole-exome sequencing improved the diagnostic yield for nuclear pedigrees with neurodevelopmental disorders. *Mol. Genet. Genomic Med.* *10*, e1918. <https://doi.org/10.1002/mgg3.1918>.
22. Ding, K., de Andrade, M., Manolio, T.A., Crawford, D.C., Rasmussen-Torvik, L.J., Ritchie, M.D., Denny, J.C., Masys, D.R., Jouni, H., Pachecho, J.A., et al. (2013). Genetic variants that confer resistance to malaria are associated with red blood cell traits in African-Americans: an electronic medical record-based genome-wide association study. *G3* *3*, 1061–1068. <https://doi.org/10.1534/g3.113.006452>.
23. Wang, K., Li, M., Hadley, D., Liu, R., Glessner, J., Grant, S.F.A., Hakonarson, H., and Bucan, M. (2007). PennCNV: An integrated hidden Markov model designed for high-resolution copy number variation detection in whole-genome SNP genotyping data. *Genome Res.* *17*, 1665–1674. <https://doi.org/10.1101/gr.6861907>.
24. Abyzov, A., Urban, A.E., Snyder, M., and Gerstein, M. (2011). CNVnator: An approach to discover, genotype, and characterize typical and atypical CNVs from family and population genome sequencing. *Genome Res.* *21*, 974–984. <https://doi.org/10.1101/gr.114876.110>.
25. Klambauer, G., Schwarzbauer, K., Mayr, A., Clevert, D.-A., Mitterecker, A., Bodenhofer, U., and Hochreiter, S. (2012). cn.MOPS: mixture of Poissons for discovering copy number variations in next-generation sequencing data with a low false discovery rate. *Nucleic Acids Res.* *40*, e69. <https://doi.org/10.1093/nar/gks003>.
26. Uitto, J., and Richard, G. (2004). Progress in epidermolysis bullosa: Genetic classification and clinical implications. *Am. J. Med. Genet. C Semin. Med. Genet.* *131C*, 61–74. <https://doi.org/10.1002/ajmg.c.30035>.
27. El Hachem, M., Zambruno, G., Bourdon-Lanoy, E., Ciasulli, A., Buisson, C., Hadj-Rabia, S., Diociaiuti, A., Gouveia, C.F., Hernández-Martín, A., de Lucas Laguna, R., et al. (2014). Multi-centre consensus recommendations for skin care in inherited epidermolysis bullosa. *Orphanet J. Rare Dis.* *9*, 76. <https://doi.org/10.1186/1750-1172-9-76>.
28. Fine, J.-D. (2016). Epidemiology of Inherited Epidermolysis bullosa based on incidence and prevalence estimates from the National Epidermolysis Bullosa Registry. *JAMA Dermatol.* *152*, 1231–1238. <https://doi.org/10.1001/jamadermatol.2016.2473>.
29. Kiritsi, D., Has, C., and Bruckner-Tuderman, L. (2013). Laminin 332 in junctional epidermolysis bullosa. *Cell Adh. Migr.* *7*, 135–141. <https://doi.org/10.4161/cam.22418>.
30. Kurnicka, K., Osipowicz, K., Dzikowska-Diduch, O., Wertheim-Tysarowska, K., Kowalewski, C., and Pruszczyk, P. (2020). The analysis of echocardiographic results in patients suffering from epidermolysis bullosa. *Postepy Dermatol. Alergol.* *37*, 871–878. <https://doi.org/10.5114/ada.2020.102101>.
31. Villa, C.R., Ryan, T.D., Collins, J.J., Taylor, M.D., Lucky, A.W., and Jefferies, J.L. (2015). Left ventricular non-compaction cardiomyopathy associated with epidermolysis bullosa simplex with muscular dystrophy and PLEC1 mutation. *Neuromuscul. Disord.* *25*, 165–168. <https://doi.org/10.1016/j.nmd.2014.09.011>.
32. Ryan, T.D., Ware, S.M., Lucky, A.W., Towbin, J.A., Jefferies, J.L., and Hinton, R.B. (2012). Left ventricular noncompaction cardiomyopathy and aortopathy in a patient with recessive dystrophic Epidermolysis Bullosa. *Circ. Heart Fail.* *5*, e81–e82. <https://doi.org/10.1161/circheartfailure.112.969675>.
33. Sidwell, R.U., Yates, R., and Atherton, D. (2000). Dilated cardiomyopathy in dystrophic epidermolysis bullosa. *Arch. Dis. Child.* *83*, 59–63. <https://doi.org/10.1136/adc.83.1.59>.
34. Fine, J.-D., Hall, M., Weiner, M., Li, K.-P., and Suchindran, C. (2008). The risk of cardiomyopathy in inherited epidermolysis bullosa. *Br. J. Dermatol.* *159*, 677–682. <https://doi.org/10.1111/j.1365-2133.2008.08697.x>.
35. Lara-Corrales, I., Mellerio, J.E., Martinez, A.E., Green, A., Lucky, A.W., Azizkhan, R.G., Murrell, D.F., Agero, A.L., Kantor, P.F., and Pope, E. (2010). Dilated cardiomyopathy in epidermolysis bullosa: a retrospective, multicenter study. *Pediatr. Dermatol.* *27*, 238–243. <https://doi.org/10.1111/j.1525-1470.2010.01127.x>.
36. Yenamandra, V.K., van den Akker, P.C., Lemmink, H.H., Jan, S.Z., Diercks, G.F.H., Vermeer, M., van den Berg, M.P., van der Meer, P., Pasmooij, A.M.G., Sinke, R.J., et al. (2018). Cardiomyopathy in patients with epidermolysis bullosa simplex with mutations in KLHL24. *Br. J. Dermatol.* *179*, 1181–1183. <https://doi.org/10.1111/bjd.16797>.
37. Thorolfssdottir, R.B., Sveinbjornsson, G., Sulem, P., Helgadóttir, A., Gretarsdóttir, S., Benonisdóttir, S., Magnusdóttir, A., Davidsson, O.B., Rajamani, S., Roden, D.M., et al. (2017). A missense variant in PLEC increases risk of atrial fibrillation. *J. Am. Coll. Cardiol.* *70*, 2157–2168. <https://doi.org/10.1016/j.jacc.2017.09.005>.
38. Cassa, C.A., Akle, S., Jordan, D.M., and Rosenfeld, J.A. (2017). When “N of 2” is not enough: integrating statistical and

- functional data in gene discovery. *Mol. Case Stud.* 3, a001099. <https://doi.org/10.1101/mcs.a001099>.
39. Lin, C.-J., Lin, C.-Y., Chen, C.-H., Zhou, B., and Chang, C.-P. (2012). Partitioning the heart: mechanisms of cardiac septation and valve development. *Development* 139, 3277–3299. <https://doi.org/10.1242/dev.063495>.
40. Gaussin, V., Morley, G.E., Cox, L., Zwijsen, A., Vance, K.M., Emile, L., Tian, Y., Liu, J., Hong, C., Myers, D., et al. (2005). Alk3/Bmpr1a receptor is required for development of the atrioventricular canal into valves and annulus fibrosus. *Circ. Res.* 97, 219–226. <https://doi.org/10.1161/01.res.0000177862.85474.63>.
41. Utriainen, A., Sormunen, R., Kettunen, M., Carvalhaes, L.S., Sajanti, E., Eklund, L., Kauppinen, R., Kitten, G.T., and Pihlajaniemi, T. (2004). Structurally altered basement membranes and hydrocephalus in a type XVIII collagen deficient mouse line. *Hum. Mol. Genet.* 13, 2089–2099. <https://doi.org/10.1093/hmg/ddh213>.
42. Lundgren, E., Gullberg, D., Rubin, K., Borg, T.K., Terracio, M.J., and Terracio, L. (1988). In vitro studies on adult cardiac myocytes: attachment and biosynthesis of collagen type IV and laminin. *J. Cell. Physiol.* 136, 43–53. <https://doi.org/10.1002/jcp.1041360106>.
43. Yang, H., Borg, T.K., Liu, H., and Gao, B.Z. (2015). Interactive relationship between basement-membrane development and sarcomerogenesis in single cardiomyocytes. *Exp. Cell Res.* 330, 222–232. <https://doi.org/10.1016/j.yexcr.2014.08.020>.
44. Abrahamson, D.R., Prettyman, A.C., Robert, B., and St John, P.L. (2003). Laminin-1 reexpression in Alport mouse glomerular basement membranes. *Kidney Int.* 63, 826–834. <https://doi.org/10.1046/j.1523-1755.2003.00800.x>.
45. Hansen, T.S., Bubb, K.J., Schiattarella, G.G., Ugander, M., Tan, T.C., and Figtree, G.A. (2022). High-resolution transthoracic echocardiography accurately detects pulmonary arterial pressure and decreased right ventricular contractility in a mouse model of pulmonary fibrosis and secondary pulmonary hypertension. *J. Am. Heart Assoc.* 11, e018353. <https://doi.org/10.1161/jaha.120.018353>.
46. Addetia, K., Yamat, M., Mediratta, A., Medvedofsky, D., Patel, M., Ferrara, P., Mor-Avi, V., and Lang, R.M. (2016). Comprehensive two-dimensional interrogation of the tricuspid valve using knowledge derived from three-dimensional echocardiography. *J. Am. Soc. Echocardiogr.* 29, 74–82. <https://doi.org/10.1016/j.echo.2015.08.017>.